

Study of Corrosion Behavior of a 2507 Super Duplex Stainless Steel: Influence of Quenched-in and Isothermal Nitrides

Eleonora Bettini^{1,*}, Ulf Kivisäkk², Christofer Leygraf¹, Jinshan Pan¹

¹KTH Royal Institute of Technology, School of Chemical Science and Engineering, Department of Chemistry, Div. of Surface and Corrosion Science, Drottning Kristinas väg.51, SE-100 44 Stockholm, Sweden

²AB Sandvik Materials Technology, SE-811 81 Sandviken, Sweden

*E-mail: bettini@kth.se

Received: 22 August 2013 / Accepted: 19 September 2013 / Published: 15 November 2013

Precipitation of different types of chromium nitrides may occur during processing of super duplex stainless steels, affecting the properties of the material. In this study the influence of quenched-in (size range ca. 50-100 nm) and isothermal (size range ca. 80-250 nm) types of nitrides on the corrosion behavior of a 2507 super duplex stainless steel has been investigated at room temperature and at 90 °C (above the critical pitting temperature) in 1 M NaCl solution. The microstructure has been characterized by scanning electron microscopy and magnetic force microscopy. The isothermal nitrides exhibit a higher Volta potential compared to the matrix, but such difference could not be observed for the quenched-in nitrides. In-situ electrochemical AFM measurements at room temperature show stable surfaces for a wide range of applied potentials despite the presence of either type of nitrides. In the transpassive region isothermal nitrides appear to be slightly more deleterious than quenched-in nitrides. At 90 °C isothermal nitrides largely reduce the corrosion resistance of the austenite phase, while the quenched-in nitrides reduce the corrosion resistance of the material to a much lesser extent. The size difference between isothermal and quenched-in chromium nitrides may be crucial, in particular above the critical pitting temperature.

Keywords: Duplex stainless steel, nitrides, exposure temperature, atomic force microscopy, corrosion

1. INTRODUCTION

Duplex stainless steels (DSSs) have a heterogeneous microstructure consisting of approximately equal amount of ferrite (α) and austenite (γ), obtained by controlling chemical composition and heat treatments, which confers excellent mechanical properties and corrosion resistance to the material [1,2]. The final products made of DSSs might during their service be

subjected to welding and/or heat treatment processes, which could lead to microstructure changes. In fact, the exposure to high heat treatment temperatures (between 500-1200 °C) could result in a different proportion of the main duplex phases and an enhanced risk of secondary phase precipitations [3]. In practice, thermodynamic calculations are commonly used to predict the constitution and amount of equilibrium phases at specific heat treatment temperatures [4].

Nitrogen is commonly added into DSSs because it is beneficial for the mechanical strengthening, the corrosion resistance of the material and for the equilibrium balance of ferrite and austenite [5]. Chromium nitrides, which are among the possible secondary phases that can precipitate in the DSSs, have become an important issue with the increasing use of high chromium and high nitrogen contents in modern DSSs [6,7]. The formation of chromium nitrides takes place during isothermal heat treatments at elevated temperatures (700-900 °C), or during the fast cooling process from the solution annealing temperatures due to the supersaturation of nitrogen in the ferritic phase [6]. Heat treatment temperature, exposure time, cooling speed and alloy composition are just some of the factors influencing the nature of the precipitating chromium nitrides, which might have different impact on the corrosion and mechanical properties of the final products [8-11]. Two families of chromium nitrides, quenched-in and isothermal, can be formed in duplex stainless steels after specific heat treatments [12-14].

Quenched-in chromium nitrides are normally formed by a fast cooling process from temperatures above ca. 1000 °C, nucleating intragranularly in the ferrite grains. In this case, the fast cooling procedure doesn't allow the nitrogen present in the ferrite phase to diffuse towards the austenite phase, which has higher solubility for nitrogen. As a consequence, the ferrite will become supersaturated in nitrogen, and very small intragranular chromium nitrides, often called "quenched-in nitrides" [14], will precipitate and finely disperse in the ferrite grains. Instead, isothermal heat treatments in the range about 700-900 °C usually result in the precipitation of intergranular chromium nitrides, often called "isothermal nitrides" [14], along the α/γ and α/α boundaries [15]. The exposure time at these elevated temperatures strongly influences the size and the amount of the nucleated isothermal chromium nitrides. In this case, nitrogen had diffused from the ferrite towards the austenite, favoring their precipitation along the α/γ and α/α boundaries [14].

Sigma phase (σ) is also one of the secondary phases that can nucleate and grow after relatively long holding time during the same heat treatment [16]. The precipitation of σ phase can be represented by a eutectoid reaction ($\alpha \rightarrow \sigma + \gamma_2$) where ferrite phase is transformed into σ phase, which is enriched in Cr and Mo, and γ_2 phase (secondary austenite), which can be depleted in Cr and Mo [1,16]. The nucleation of σ phase generally starts at the α/γ boundaries and proceeds towards the ferrite phase until its complete transformation [16].

It has been reported that chromium nitrides and other secondary precipitated phases may have deleterious effects on the corrosion resistance of DSSs, due to the formation of Cr-depleted zones in their surrounding area [7]. In a previous study, a corrosion tendency evaluation of a DSS suggested a larger detrimental effect of isothermal nitrides on the corrosion resistance of the material compared to quenched-in nitrides [14]. Because of the great importance of the effect of chromium nitrides on the performances of super DSSs, further studies are necessary to gain a deeper understanding of the

influence of different types of chromium nitrides on the corrosion behavior of the DSSs at different exposure temperatures.

In this paper, we report the results from a detailed study on two differently heat treated samples of a super duplex stainless steel (SDSS) 2507 with high contents of chromium and nitrogen, with the focus to compare the effect of quenched-in and isothermal types of chromium nitrides on the corrosion behavior of the material. Thermodynamic calculations were performed to predict the formation of the nitrides. Scanning electron microscopy (SEM) and magnetic force microscopy (MFM) were used to characterize the microstructure and the precipitated phases. Kelvin force microscopy (KFM) was used to evaluate the relative nobility of the nitrides precipitated in the SDSS. Electrochemical potentiodynamic polarization measurements at room temperature and above the critical pitting temperature (CPT) of the material, in-situ electrochemical atomic force microscopy (EC-AFM) measurements as well as post-polarization analyses were performed to investigate the effect of the two types of chromium nitrides on the passivity and localized corrosion behavior of the heat treated 2507 SDSS samples.

2. EXPERIMENTAL

2.1. Material and sample preparation

Samples of a 2507 SDSS (UNS S32750) were commercially produced as plate material and solution annealed in the production process. The chemical composition of the material is shown in Table 1.

Table 1. Chemical composition of the tested material (wt %).

C	Si	Mn	P	S	Cr	Ni	Mo	Cu	N	Fe
0.015	0.24	0.83	0.023	0.001	24.8	6.89	3.83	0.23	0.27	Bal.

Subsequent heat treatments were performed at Swerea KIMAB, Sweden, at two different temperatures, in order to precipitate different types of chromium nitrides: 1125 °C for 10 min and 800 °C for 10 min, respectively, followed by water quenching. The two heat treatment temperatures were carefully selected after thermodynamic calculation of the equilibrium phases by mean of Thermo-Calc [17,18] and TCFE6 database (Fig. 1).

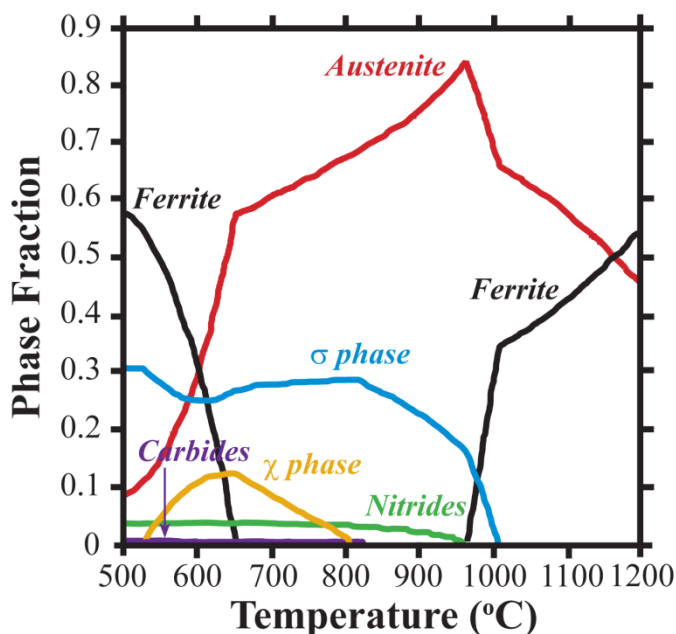


Figure 1. Thermodynamic calculation of equilibrium phases vs. heating temperature.

As can be observed in Figure 1, by holding the temperature at 1125 °C austenite and ferrite are the only phases found at thermodynamic equilibrium. At this temperature the material should be free from precipitated nitrides, but due to the subsequent fast water quenching process, the nitrogen present in the ferrite doesn't have enough time to diffuse towards the austenite, precipitating instead as quenched-in nitride particles finely dispersed in the ferrite grains [14]. This sample from now on is denoted 2507 QUE.

For the sample heat treated at 800 °C, Figure 1 shows that the equilibrium phases are austenite, σ phase and chromium nitrides. The amount, size, location and distribution of these secondary phases may vary with the holding time at this temperature. Since the eutectoid decomposition of ferrite into σ phase at 800 °C takes several tens of hours to be completed [19,20], during the 10 min heating at 800 °C, just a small percentage of the ferrite could be transformed into σ phase and γ_2 . Meanwhile, the nitrogen present in the ferrite had enough time to diffuse towards the austenite, thus isothermal nitrides have nucleated along the α/γ and α/α boundaries and their size was determined by the heating time [15]. This sample from now on is denoted 2507 ISO.

The samples used for the SEM characterization, with dimensions of 10×10×5 in mm, were wet ground with SiC papers and further polished with diamond paste up to 0.25 μm . Due to the small size of the quenched-in nitrides, the 2507 QUE sample was gently etched (electrolytical etching in 30 vol% HNO_3 at 2 volts for 5 seconds). Note that the etching procedure was done only for the preliminary SEM characterization of this sample.

Prior the MFM and KFM measurements, 2507 QUE and 2507 ISO samples, with dimensions of 10×10×2 in mm, were wet ground with SiC papers and further polished with diamond paste up to 0.25 μm . The samples used for potentiodynamic polarization measurements were successively polished with diamond paste up to 1 μm . The small samples used for the in-situ EC-AFM

measurements were cut from the received square samples and mounted on a brass disc by conductive silver paint. The samples were then fixed in a plastic mold by epoxy, leaving an exposed area of 0.2 cm², and underwent the same preparation procedures as for the MFM and KFM measurements. All samples, including those used for the post-polarization analyses, were ultrasonically cleaned in ethanol and dried with N₂ gas stream.

2.2. Solution

The 1 M NaCl solution used in this study was prepared from analytical grade NaCl and ultrapure water (Milli-Q, 18 MΩ cm).

2.3. SEM characterization

The microstructures of the 2507 QUE and 2507 ISO samples were characterized by using a JEOL JSM-7000F field emission SEM. To detect the very small quenched-in nitrides in the 2507 QUE sample, the gently etched sample surface was imaged by secondary electron (SE) mode. Instead, due to the larger size of the isothermal nitrides formed in the 2507 ISO sample, their detection was easily done on the polished surface by backscattering electron (BSE) mode imaging.

2.4. MFM measurements

The MFM measurements were performed on the polished surfaces of the 2507 QUE and 2507 ISO samples in order to characterize and identify the main duplex phases, ferrite and austenite. A Dimension 3100 AFM from Veeco was used for the MFM imaging and probes of the MESP type with CoCr magnetic coating (resonance frequency 60-100 kHz, spring constant 1-5 N/m), purchased from Bruker, were used for the measurements. The images were recorded by using 512 points/line with a scan rate of 0.5 Hz. A dual-scan lift mode was used to obtain concurrent topography and magnetic images of the same scanned area. The signal from the topography was recorded during the first line scan, while the magnetic signal was recorded in the second pass where the tip was lift approximately 50 nm from the surface in order to avoid cross-talking disturbances. The magnetic domains of the two materials were displayed in the phase image with a scale unit expressed in degree (deg).

2.5. KFM measurements

The KFM measurements were performed by using an Agilent 5500 scanning probe microscope equipped with a MAC III unit. This system has three lock-in amplifiers able to run multi-frequency measurements. The topography and Volta potential signals were simultaneously recorded by using a single-pass mode to achieve a high lateral resolution. The principle of the technique and the details of the instrumental setup have been previously described [21,22]. The probes used for these measurements were Nanoprobes of SCM-PIT type purchased from Bruker, having a resonance

frequency of 60-100 kHz, a spring constant of 1-5 N/m and a conductive coating (PtIr) necessary for measuring the electrical signal.

2.6. Electrochemical instrument and measurements

Potentiodynamic polarization measurements were performed to investigate passivity, corrosion/dissolution behavior and eventual breakdown of the 2507 QUE and 2507 ISO samples, in 1 M NaCl solution at room temperature (T_{room} , ca. 20 °C) and 90 °C, which is above the CPT values of both the 2507 QUE and 2507 QUE samples [14].

A Solartron 1287 electrochemical interface was used for the potentiodynamic polarization measurements. An Avesta Cell purchased from Bank Elektronik was used as three electrode cell, with the sample as working electrode, a saturated Ag/AgCl electrode (197 mV vs. SHE) as reference electrode and a platinum mesh as counter electrode. The Avesta cell is specially designed for avoiding crevice corrosion due to mounting of the sample onto the cell. An external thermostat was connected to the heating jacket of the Avesta cell, allowing the control of the electrolyte temperature. The solution was added in the amount of ca. 300 mL and the exposed sample area was of 1 cm². The open circuit potential (OCP) was recorded for 15 min, followed by the potentiodynamic polarization measurement, in which the potential was swept from -0.2 V vs. OCP towards more positive potential values with a constant rate of 0.5 mV/s.

2.7. In-situ EC-AFM measurements

The in-situ EC-AFM measurements were performed to investigate the corrosion/dissolution behavior of the 2507 QUE and 2507 ISO samples in the NaCl solution, through monitoring the topographic changes taking place at consecutive applied anodic potentials at T_{room} . The AFM instrument used was an Agilent 5500 scanning probe microscope equipped with a MAC III unit and a built-in potentiostat. The electrochemical cell used was specially designed for this application. The instrumental details have been described elsewhere [23]. The SDSS samples were the working electrode, a saturated Ag/AgCl electrode (197 mV vs. SHE) was used as reference electrode and a platinum sheet as counter electrode. The 1M NaCl solution was added into the cell so that the sample surface was covered by a solution layer of ca. 3 mm thickness. The probes used for the contact mode AFM were ContAl-G silicon AFM probes, purchased from Budget Sensor, with a resonance frequency of 13 kHz and a spring constant of 0.2 N/m.

2.8. Post-polarization investigation

Light optical microscopy investigation was performed on the corroded surfaces of the 2507 ISO and 2507 QUE samples after the polarization measurements at 90 °C, rinsing with ethanol and drying with N₂ gas stream.

3. RESULTS AND DISCUSSION

3.1. SEM characterization

The duplex structure and secondary phases (chromium nitrides and σ phase) formed in the samples due to the heat treatments were revealed by the SEM imaging in suitable modes. Figure 2a-b gives an example of backscattered images showing the typical elongated duplex structure for the 2507 QUE and 2507 ISO samples. Austenite exhibits brighter contrast in the BSE mode, compared to ferrite, which appears darker [14]. Small islands of austenite can be generally observed in the ferrite grains of both samples, but with higher visibility in the 2507 ISO. Figure 2c displays a SE image with a typical ferrite phase of the 2507 QUE sample with finely dispersed quenched-in nitrides. Due to the small dimension, their detection by high resolution SEM was possible only on a gently etched surface. Acicular, round and speckled shaped nitrides can be observed, with a size range of ca. 50-100 nm [14]. The austenite, instead, appears free from secondary phase precipitates. In Figure 2d typical isothermal nitrides precipitated along the α/γ boundaries in the 2507 ISO sample can be clearly observed on the freshly polished surface without etching. They appear darker in the BSE-SEM image (black spots) due to the high content of N, and present larger dimension, with a size range of ca. 80-250 nm [14], compared to the quenched-in nitrides. Moreover, a small amount of sigma phase particles can also be observed in Figure 2b, typically precipitated along the α/γ boundaries, exhibiting brighter contrast (white spots) in the BSE-SEM image due to its higher content in Mo. The small amount of sigma phase found in the material is due to the short exposure time (10 min) during heat treatment at 800 °C, which limited the extent of transformation of ferrite to σ phase.

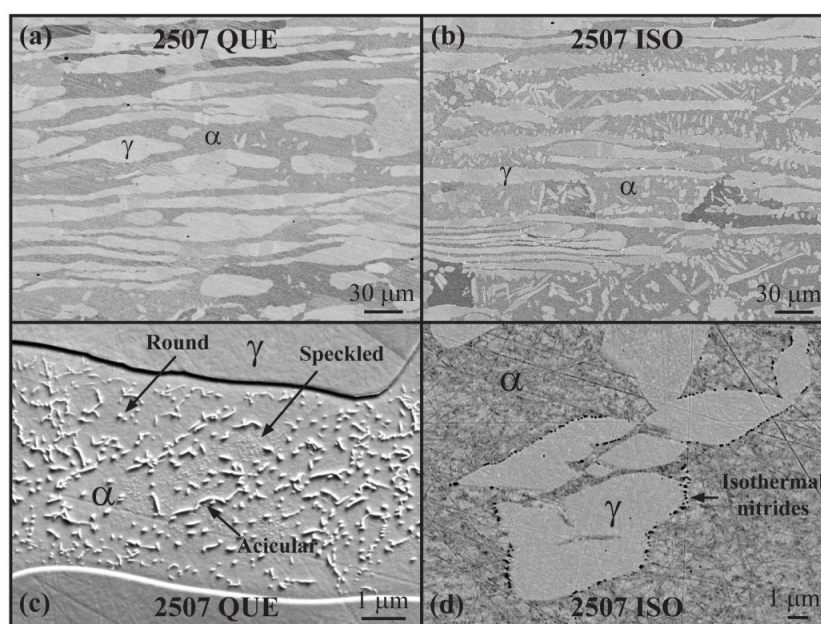


Figure 2. a-b) BSE micrographs of typical elongated duplex structure for the 2507 QUE and 2507 ISO samples (limited amount of sigma phase, white spots, in 2507 ISO), respectively. c) SE micrograph of the 2507 QUE sample (etched), showing finely dispersed nano-sized quenched-in nitrides in the ferrite grains. d) BSE micrograph of the 2507 ISO sample, showing isothermal nitrides, appearing black in the backscattering mode, precipitated along α/γ boundaries.

3.2. MFM characterization

Figure 3a-b shows the magnetic domain distributions of the unetched 2507 QUE and 2507 ISO samples, respectively. The magnetic domains obtained by MFM give a direct information of the ferrite and austenite location in the material [24]. In fact, the ferrite phase, being ferromagnetic, exhibits a “worm” like striped magnetic pattern due to the presence of different magnetic domains, whereas the austenite, being paramagnetic, exhibits a rather uniform contrast in both samples. The differences in the contrast within the ferrite phase are most likely due to different crystallographic and domain orientations [24]. It can be observed that a large number of rather small austenite islands have been formed within the ferrite matrix in both materials, with a larger extent in the 2507 ISO sample.

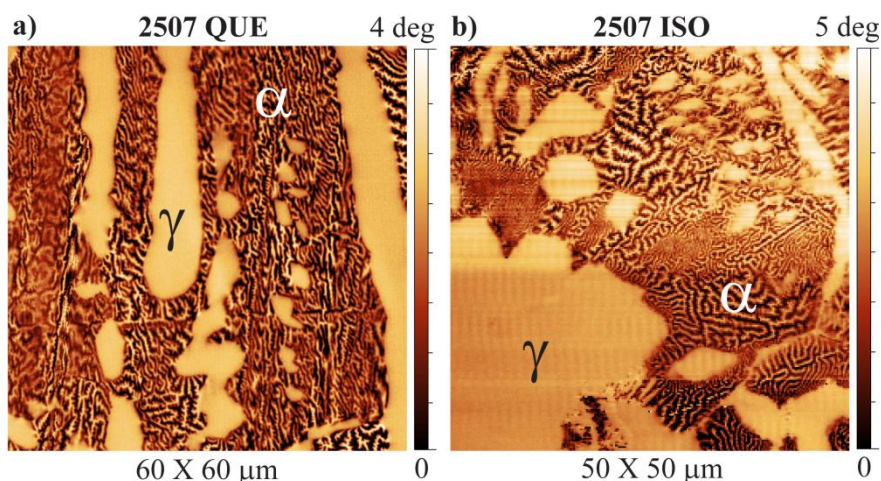


Figure 3. MFM domain images showing the typical “worm” like magnetic pattern of the ferrite (α) and the uniform contrast of the austenite (γ) in **a)** 2507 QUE and **b)** 2507 ISO samples.

3.3. KFM characterization

By using the single-pass multi-frequency technology in the KFM measurements, a higher resolution has been achieved in the Volta potential mapping compared to previous studies [14,18,24]. Figures 4a-d display examples of Volta potential maps obtained in air at T_{room} for the polished SDSS 2507 QUE and 2507 ISO samples.

In the 2507 QUE sample, the austenite phase generally exhibits slightly higher Volta potential (brighter contrast) in the images (Fig. 4a-b), suggesting its slightly higher relative nobility compared to the ferrite phase. Some local Volta potential variations can be observed within both phases, which may be due to differences in local elemental composition, different crystallographic orientations, or in the case of the ferrite grains different amounts of the small quenched-in nitrides. In this case the sample surface was polished without any etching, thus the very small quenched-in nitrides were not visible in the topography, and their presence could not be resolved in the Volta potential images. The limitation of this technique in displaying the Volta potential difference of nano-sized nitrides has been investigated elsewhere [14]. On the other hand, these results suggest that the presence of finely dispersed quenched-in nitrides in the ferrite doesn't significantly affect the corrosion tendency of the

material. The very small dimension of the finely dispersed quenched-in nitrides seems not to create large Cr and N depletions in their surrounding areas, probably due to their fast nucleation and limited growth during the rapid cooling process. Instead, the α/γ phase boundaries show the darkest contrast in the Volta potential images, indicating these sites as more prone to corrode in case of aggressive conditions. This might be due to alloying element depletion at the α/γ phase boundaries, caused by the partitioning of key alloying elements between austenite and ferrite, observed even for commercial grade duplex stainless steels, free from precipitated nitrides [25,26].

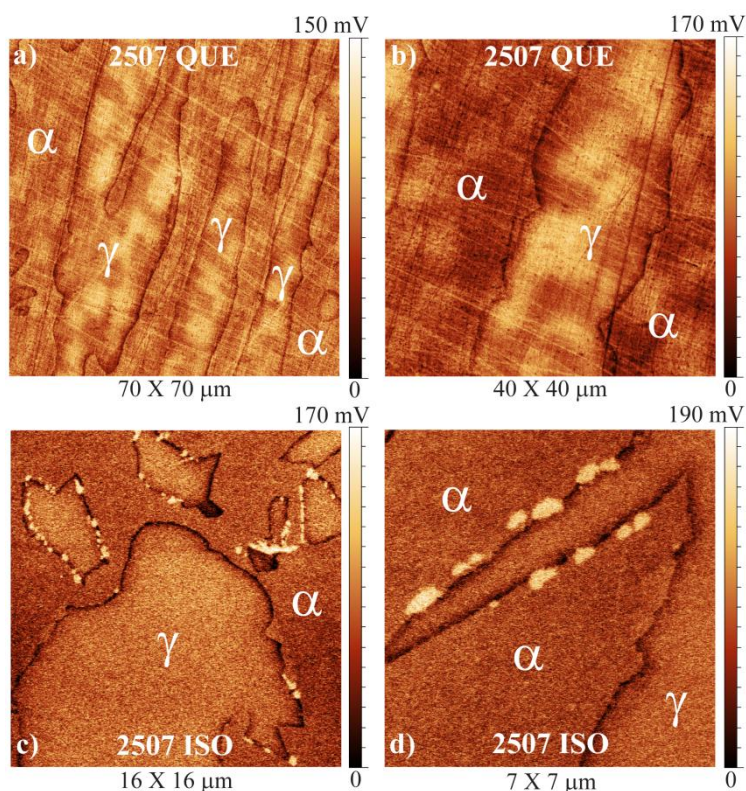


Figure 4. (a, b) Volta potential maps of the 2507 QUE sample showing different nobility between austenite (γ) and ferrite (α) phases, and (c, d) Volta potential maps of the 2507 ISO sample showing higher nobility of the isothermal nitrides (bright contrast) and lower nobility of the α/γ boundaries (dark contrast).

For the 2507 ISO sample, the highest Volta potential areas (bright sites in Fig. 4c-d) clearly show the isothermal nitrides precipitated along the α/γ phase boundaries. The precipitated nitrides exhibit higher relative nobility when compared to both the ferrite and the austenite, in agreement with previous observations [14]. Note that the sample surface was just polished without being etched. In this case, although the nitrides were not visible in the topography images, they could be easily identified in the Volta potential images because of their significantly higher Volta potential compared to the surrounding areas. The low Volta potential observed at the phase boundaries (dark contrast) suggests these sites as locations susceptible to localized corrosion initiation. The low potential of the phase boundaries could be due either to alloying element depletion caused by the formation of the

precipitates, or to the presence of γ_2 . It has been reported that γ_2 easily forms along the α/γ phase boundaries in a temperature range at which isothermal nitrides precipitate in SDSS 2507 [27,28]. γ_2 has lower Cr, Mo and N contents compared to the primary austenite [27], especially when cooperatively precipitates with chromium nitrides, and therefore more susceptible to corrosion initiation [15]. The effect of γ_2 on the corrosion behavior of DSS is a topic for another study.

σ phase was not observed in the Volta potential maps of the 2507 ISO sample, due to its small amount in the material.

3.4. Influence of quenched-in and isothermal nitrides on the dissolution initiation at room temperature

Potentiodynamic polarization measurements were carried out for the 2507 QUE and 2507 ISO samples exposed to 1 M NaCl solution at T_{room} , and Figure 5 displays typical polarization curves obtained for the two materials under these conditions.

At T_{room} , both samples exhibit high corrosion resistance, with rather similar behavior, showing a wide passive range (up to 1.2 V_{Ag/AgCl}) and a passive current density below the order of $\mu\text{A}/\text{cm}^2$, in which a protective passive film is formed on the sample surface, reducing the dissolution rate and protecting the material from corrosion attack. Despite the presence of finely dispersed quenched-in nitrides in the ferrite phase of the 2507 QUE sample and isothermal nitrides, together with a small amount of σ phase, in the 2507 ISO sample, these results indicate the preservation of the high corrosion resistance of the investigated materials when exposed to 1 M NaCl at T_{room} .

The presence of nitrides, either quenched-in or isothermal type, did not cause the onset of a localized corrosion attack at T_{room} , a result already observed for a heat treated 2205 DSS with precipitated quenched-in nitrides that will soon be published.

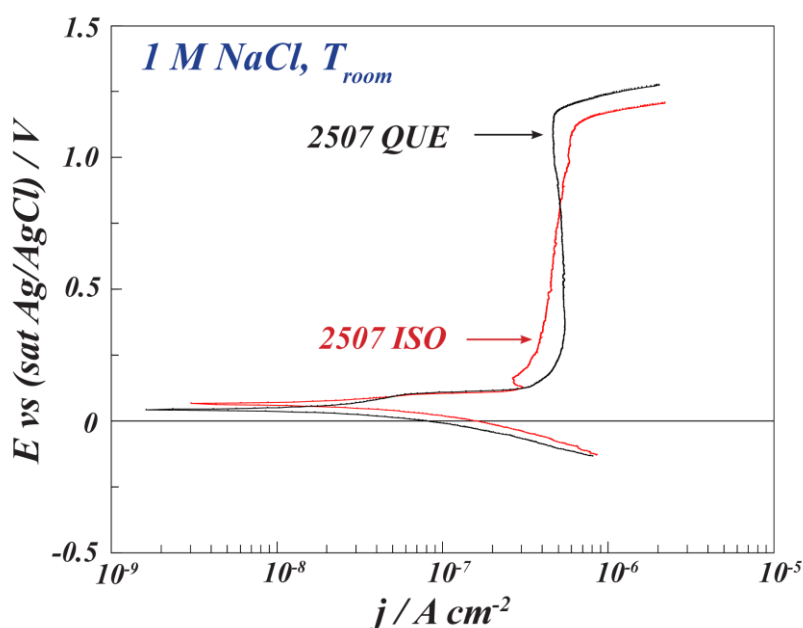


Figure 5. Potentiodynamic polarization curves for the 2507 ISO and 2507 QUE samples, when immersed in 1 M NaCl at T_{room} , with a scan rate of 0.5 mV/s.

At anodic potential higher than $1.2 V_{Ag/AgCl}$ (extreme condition, not possible in practice without external polarization) a current increase is registered for both samples, due to the transpassive dissolution of the material together with the water oxidation reaction. Unfortunately, potentiodynamic polarization measurements provide just information on the overall corrosion behavior of a material. In order to gain a deeper knowledge on the sites for dissolution initiation at high anodic potential, an in situ EC-AFM investigation was executed.

In situ EC-AFM measurements were performed for the 2507 QUE and 2507 ISO samples in 1 M NaCl solution at T_{room} at stepwise increased applied potentials. Figures 6a-c and 7a-c show examples of topographic changes due to the increasing of the anodic potential for the two samples. At the OCP conditions (Fig. 6a and Fig. 7a) and at the anodic polarization in the passive range up to $1.1 V_{Ag/AgCl}$ (Fig. 6b and Fig. 7b), the surfaces of the two samples remained to be very stable, where no topographic changes could be detected by repeated AFM imaging. In fact, due to the well polished surfaces, even the identification of the ferrite and austenite phases is a difficult task. These observations indicate a stable passive behavior of the two materials in this concentrated chloride solution (1 M NaCl). This implies that at T_{room} the presence of precipitated chromium nitrides, either a large amount of finely dispersed nano-sized quenched-in nitrides or slightly larger isothermal nitrides, together with a small amount of σ phase, doesn't have a large negative effect on the corrosion resistance of the 2507 SDSS without application of a high potential. The results indicate that both the ferrite and the austenite phases of this highly alloyed SDSS form a stable protective passive film on the surface.

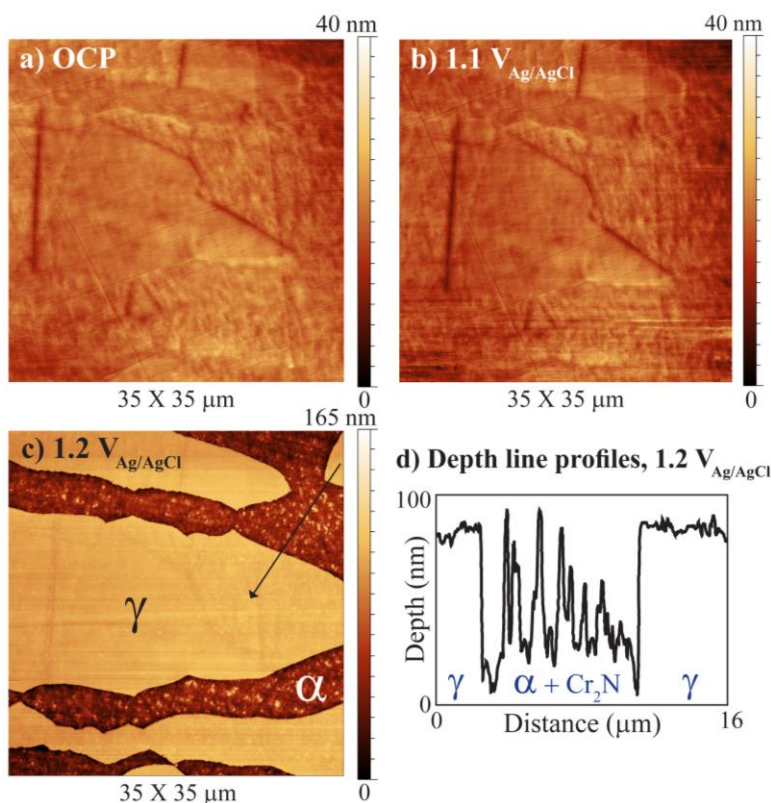


Figure 6. In situ AFM images of the same area of 2507 QUE sample obtained under potential control in 1 M NaCl solution at T_{room} : **a)** at OCP, **b)** $1.1 V_{Ag/AgCl}$, **c)** at $1.2 V_{Ag/AgCl}$. **d)** Depth line profile drawn at $1.2 V_{Ag/AgCl}$, for the line marked in Fig. 6c.

Some topographic changes started to be detected at $1.2 V_{Ag/AgCl}$, where transpassive dissolution of the samples surfaces occurred. At this high anodic potential, the two samples exhibited different dissolution behaviors. From Figure 6c it can be noted that the dissolution process of the 2507 QUE sample initiated in the ferrite phase, appearing like selectively etched, while some small particles in the ferrite phase became visible, remaining in the dissolving matrix. Figure 6d shows the depth line profile for the 2507 QUE sample polarized at $1.2 V_{Ag/AgCl}$ (line shown in Fig. 6c), where the protruding particles presents a height of ca. 90 nm compared to the dissolved matrix. These particles are identified as the quenched-in nitrides, judging from their position, dispersion, size and stability (relative nobility). Preferential dissolution can also be observed along the α/γ boundaries in the line profile in Figure 6d. The higher susceptibility of the ferrite phase and α/γ boundaries to undergo preferential dissolution at high anodic potential is in accordance with the KFM results previously reported (Fig 4a and 4b).

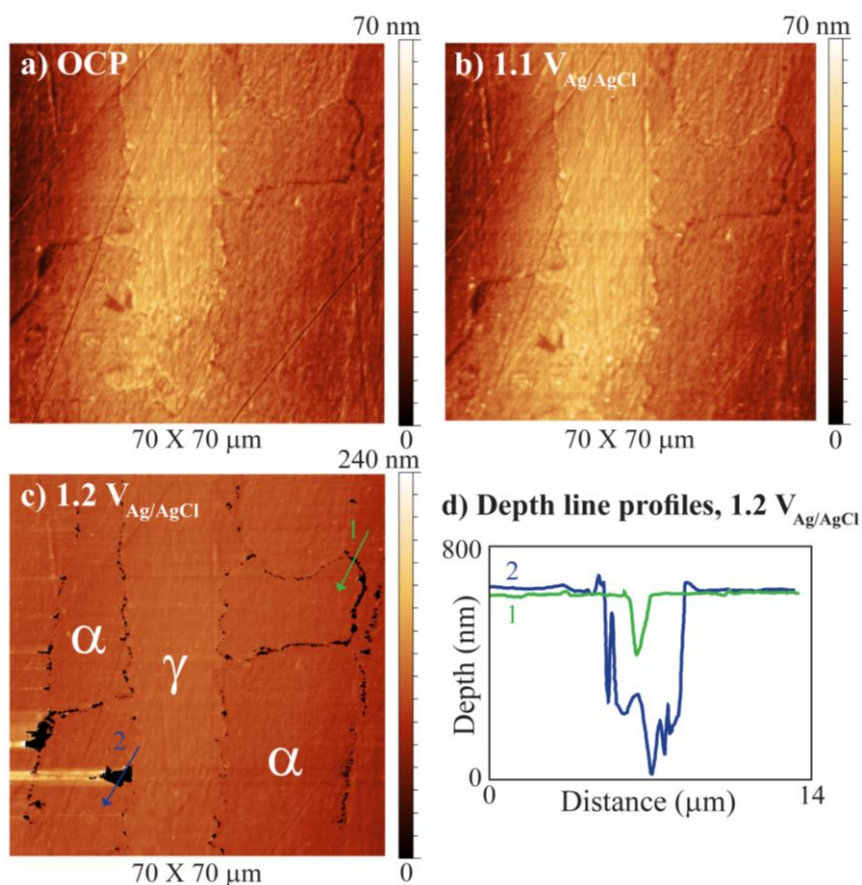


Figure 7. In situ AFM images of the same area of 2507 ISO sample obtained under potential control in 1 M NaCl solution at T_{room} : **a)** at OCP, **b)** $1.1 V_{Ag/AgCl}$, **c)** at $1.2 V_{Ag/AgCl}$. **d)** Depth line profile at $1.2 V_{Ag/AgCl}$, for the lines marked in Fig. 7c.

Different is the behavior of the 2507 ISO sample during transpassive dissolution at $1.2 V_{Ag/AgCl}$, where no selective dissolution of the ferrite phase was observed, and both austenite and ferrite remained rather stable under this condition. Instead, the dissolution process initiated and took place mainly along the α/γ phase boundaries (Fig. 7c), situation observed also in previous studies [15,27-31].

As shown in the SEM images (Fig. 2 b,d), a number of isothermal nitrides and a small amount of σ phase had precipitated along the γ/α phase boundaries in the 2507 ISO sample. These secondary phases are enriched in alloying elements (mostly Cr, Mo and N) [32,33], which are subtracted from the surrounding areas during their nucleation and growth, creating alloying elemental depleted zones [7] that may become the starting points for metal dissolution under highly corrosive conditions. This explains the localized transpassive dissolution that selectively occurred in the boundary regions surrounding the isothermal nitrides and the σ phase. With prolonged polarization at the potential of 1.2 $V_{Ag/AgCl}$ (> 20 min), the metal dissolution in these locations became so severe that even these precipitated particles had been detached from the surface.

Figure 7d displays the depth profiles of two lines (lines shown in Fig. 7c) drawn on the surface of the 2507 ISO sample after 30 minutes of holding potential at 1.2 $V_{Ag/AgCl}$. Line 1 crosses a selectively corroded α/γ phase boundary with a dissolution depth of ca. 200 nm, where most probably nano-sized isothermal nitrides were present and caused local alloying element depletion in their boundary regions. Line 2 crosses a micron-sized selectively dissolved area with a dissolution depth of ca. 650 nm, where most likely σ phase was located, possibly together with γ_2 .

Also in this case, the dissolution behavior of the 2507 ISO sample at transpassive conditions is in accordance with the Volta potential mapping results (Fig. 4c-d), and indicates the nearby areas of the isothermal nitrides and the α/γ boundaries as the sites more prone to undergo anodic dissolution at T_{room} .

The quenched-in nitrides present in the 2507 QUE sample, due to their small size (ca. 50-100 nm) and uniform dispersion, did not cause considerable alloying element depletion in the ferrite phase, which might have led to local breakdown of the passive film at T_{room} . The same phenomenon was observed on a previous and soon published study on a heat treated 2205 DSS. This common observation indicates that size and distribution of the precipitated nitrides are important for the corrosion/dissolution resistance, and the nano-sized finely dispersed quenched-in nitrides are not harmful for the DSSs with sufficient contents of Cr, Ni and Mo.

For the 2507 ISO sample, the presence of the isothermal nitrides together with a small amount of σ phase didn't cause localized corrosion of this SDSS at T_{room} . The precipitation of the isothermal nitrides and a small amount of σ phase particles along the α/γ phase boundaries can cause some alloying element depletion in the boundary area [24]; however, the extent of the depletion is limited by the small size of these secondary phases, ensuring the maintenance of passivity and thus the corrosion resistance even in these areas. This implies that even if the precipitation of some small isothermal nitrides and a small amount of σ phase would occur during the processing or heat treatments of the final product made of the 2507 SDSS, this will not drastically decrease its corrosion resistance in chloride solution at T_{room} with no applied potential.

During transpassive dissolution at 1.2 $V_{Ag/AgCl}$ in 1 M NaCl at T_{room} , the topographic changes of the surfaces monitored by the EC-AFM revealed different behaviors of the two 2507 DSS samples, influenced by the nature, size and locations of the precipitated secondary phases. One can assume that the slight alloying element depletion in these areas may act as preferential dissolution sites under extreme conditions such as transpassive dissolution. The isothermal nitrides formed along the phase boundaries in the 2507 ISO sample seem to have a more detrimental effect on the corrosion behavior

of the material than the quenched-in nitrides in the 2507 QUE sample under transpassive conditions, causing larger dissolution depth. Note that this dissolution is induced by the application of a high anodic potential, not a normal corrosion situation.

In short, the results obtained at T_{room} indicate that the nano-sized quenched-in and isothermal nitrides are not harmful for the corrosion resistance of this SDSS in 1 M NaCl when no elevated anodic potentials are applied. Under transpassive dissolution, the quenched-in nitrides lead to selective dissolution of the ferrite, whereas the isothermal nitrides cause preferential dissolution along the α/γ boundaries, most probably due to the formation of some alloying element depletion regions in their surrounding areas.

3.5. Influence of quenched-in and isothermal nitrides on the corrosion initiation at temperature above the CPT

Potentiodynamic polarization measurements were carried out for the 2507 QUE and 2507 ISO samples exposed to 1 M NaCl solution at 90 °C, and Figure 8 displays typical polarization curves obtained for the two materials under these conditions. At 90 °C (temperature just above the earlier measured CPT of the 2507 QUE sample [14]), the 2507 QUE sample showed a wide passive potential region, with a current value in the range of $\mu\text{A}/\text{cm}^2$ up to the potential of ca. 0.8 $V_{\text{Ag}/\text{AgCl}}$. These results indicate a good corrosion resistance for the 2507 QUE sample even at this temperature (90 °C) in this concentrated chloride solution. This implies that the presence of nano-sized (ca. 50-100 nm) quenched-in nitrides finely dispersed in the ferrite grains doesn't have a large effect on the corrosion resistance of the 2507 SDSS, even at this temperature. At the applied potential of 0.8 $V_{\text{Ag}/\text{AgCl}}$ passivity breakdown occurred and a sharp increase of current density, typical for the onset of localized corrosion, was observed.

In contrast, the 2507 ISO sample didn't exhibit any passivity at 90 °C, where the current density increased gradually with the potential from the corrosion potential (ca. -0.2 $V_{\text{Ag}/\text{AgCl}}$) up to 0.08 $V_{\text{Ag}/\text{AgCl}}$, followed by a sharp current rise as a result of a fast initiation and propagation of corrosion attack.

The 2507 ISO sample is not resistant under these exposure conditions, whereas the 2507 QUE sample may still be considered to be resistant despite of a large amount of quenched-in nitrides. These results show that the presence of the isothermal nitrides (ca. 80-250 nm) and a small amount of σ phase have harmful effects on the corrosion resistance of the material at temperatures above the CPT, limiting the range of exposure temperature at which the material can be used.

In order to investigate the origin of the corrosion initiation at these conditions, a closer look of the corroded surfaces was taken by light optical microscopy. Figure 9 gives examples of the initial stages of the corrosion processes for the two materials.

For the 2507 QUE (Fig. 9a), passivity breakdown occurred at 0.8 $V_{\text{Ag}/\text{AgCl}}$, and ferrite was the phase suffering selective dissolution, which developed into pitting corrosion (black areas in the image), starting in confined spots, probably in the areas around the quenched-in nitrides, and propagating to the entire ferrite phase. Small islands of the austenite phase within the ferrite grains, similar to the previously observed in Figures 2a and 3a can be noted in the uncorroded part of the image, allowing

the identification of the two phases. BSE post-analysis investigation confirmed the preferential corrosion of the ferrite phase.

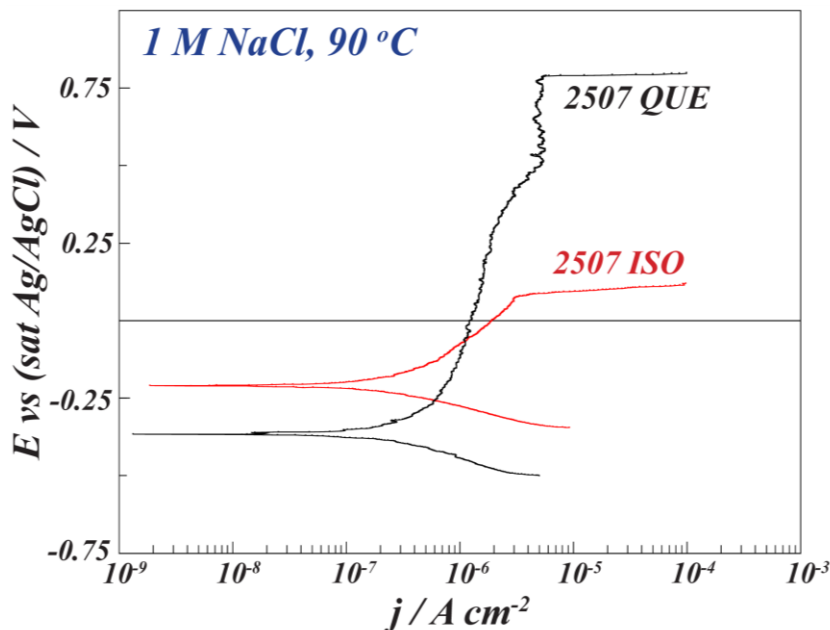


Figure 8. Potentiodynamic polarization curves for the 2507 ISO and 2507 QUE samples, when immersed in 1 M NaCl at 90 °C, with a scan rate of 0.5 mV/s.

The increase of exposure temperature from T_{room} to 90 °C resulted in a reduced passive range for the 2507 QUE sample. Nevertheless, a passive behavior up to 0.8 $V_{\text{Ag/AgCl}}$ can still be regarded as a good corrosion resistance, because under normal exposure situations (without applied potential) it is unlikely that some cathodic reactions can support the corrosion process occurring at this high potential. It should be noted that the CPT for a commercial 2507 SDSS free from precipitated secondary phases in 1 M NaCl is around 95°C [14]. It follows that the presence of quenched-in nitrides doesn't largely affect the corrosion performances of this SDSS, where the passivity and the corrosion resistance are maintained in this concentrated NaCl solution at high exposure temperatures up to at least 90 °C.

For the 2507 ISO sample, a sharp rise in current density occurred at the applied potential of 0.08 $V_{\text{Ag/AgCl}}$, and the austenite was the phase interested by corrosion initiation and propagation (Fig. 9b). In fact, also in this case small islands of austenite, similar to those previously observed in Figures 2b and 3b, can be observed within the ferrite matrix. The austenite appears now darker because of its faster dissolution, compared to the ferrite, during polarization at 90 °C. As can be noted in Figure 9b, the austenite grains exhibit different dissolution tendency, some (darker areas) are more prone to dissolve, while other (lighter areas) are slightly more resistant to corrosion. This could be related to different crystallographic orientations of the grains, which it was proved to have an influence on preferential corrosion of stainless steels [34,35]. The same phenomenon was observed, and soon published, for a heat treated 2205 DSS exposed to concentrated chloride solution at a temperature slightly above the CPT, where just some of the austenite grains were selectively dissolved.

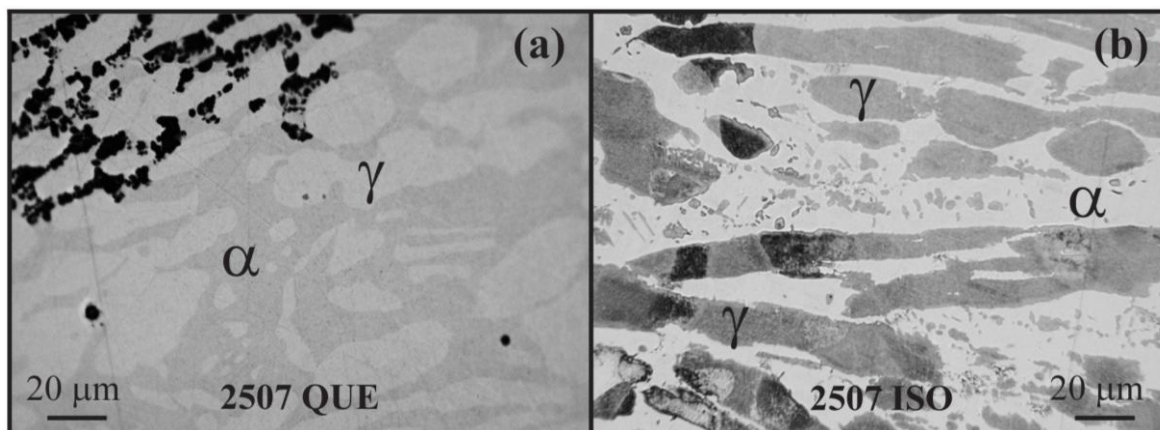


Figure 9. Light optical microscopy micrographs of the corroded areas after the onset of fast dissolution upon anodic polarization in 1 M NaCl solution at 90 °C, of **a)** 2507 QUE and **b)** 2507 ISO, respectively.

The pitting resistance equivalent (PRE) number is often used for comparing the corrosion resistance of stainless steels. This number is obtained by empirical equations, which take into account the amount of specific alloying elements, as Cr, Mo and N. The most commonly used equation (Eq. 1) is given below [27,36]:

$$\text{PRE} = (\% \text{Cr}) + 3.3 (\% \text{Mo}) + 16 (\% \text{N}) \quad (\text{Eq. 1})$$

Figure 10 shows the thermodynamic calculation by Thermo-Calc [17] of the PRE number of the specifically tested 2507 DSS, as a function of heat treatment temperature, for the ferrite and the austenite phases. It can be noted that, at the heating temperature of 1125 °C ferrite and austenite have similar PRE values, slighter higher for the ferrite phase ($\text{PRE}_\alpha \approx 43$) than the austenite ($\text{PRE}_\gamma \approx 41$). Both phases still have very high PRE values, but the thermodynamic calculation would suggest austenite as preferential phase for pitting initiation at temperatures above the CPT.

However, as shown in Figure 9a, for the 2507 QUE sample ferrite was observed to be the phase suffering preferential corrosion at temperature just above the CPT when passivity breakdown occurred. This deviation of the corrosion behavior from the thermodynamic prediction can be explained by taking into account the effect of the precipitated quenched-in nitrides. At the heating temperature of 1125 °C, nitrides are not among the stable equilibrium phases (Fig. 1), and for this reason not considered in the thermodynamic calculation of the PRE plot (Fig. 10). In reality, nano-sized quenched-in nitrides were formed in the ferrite phase of the 2507 QUE sample (Fig. 2c) due to the quick cooling. The precipitation of the quenched-in nitride particles (although very small) in the ferrite phase will subtract a certain amount of Cr and N from the matrix, thus resulting in a locally lower PRE value within the ferrite matrix. Due to the presence of a large number of quenched-in nitride particles precipitated in the ferrite phase, the PRE number of the ferrite matrix may decrease to a value lower than the PRE value of the austenite, so that the ferrite phase becomes preferential site for corrosion initiation.

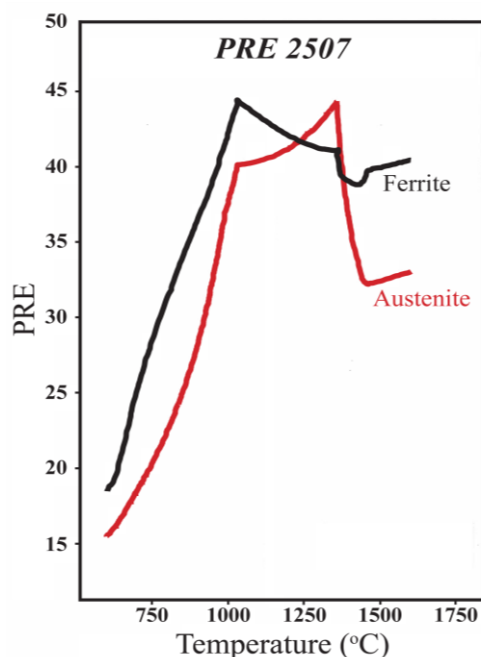


Figure 10. Thermodynamic calculation of the PRE number for the ferrite and austenite phases in the SDSS 2507.

The situation is quite different for the 2507 ISO sample. In this case, the CPT of this type of sample is ca. 77 °C [14], quite a large decrease from 95 °C for the commercial grade of the 2507 SDSS. At the exposure temperature of 90 °C, a sharp rise of the current density (fast corrosion process) occurred already at a low potential (0.08 V_{Ag/AgCl}) in 1 M NaCl, so the passivity is lost when the exposure temperature is increased from T_{room} to 90 °C. The post-polarization analysis showed that austenite was the phase preferentially corroded after the polarization up to 0.08 V_{Ag/AgCl}. The higher susceptibility of the austenite to undergo pitting corrosion can be explained by the thermodynamic calculation of the PRE values. In Figure 10 it can be seen that at the heating temperature of 800 °C, the PRE value of the ferrite (PRE_α ≈ 31) is much higher than for the austenite phase (PRE_γ ≈ 22). At 800 °C nitrides and σ phase are among the equilibrium phases considered in the thermodynamic calculation, and thus already excluded from the PRE prediction of the ferrite and the austenite in Figure 10. The lower PRE number of the austenite phase is due to its lower amount in Cr and Mo, most probably as a result of the precipitation of the isothermal nitrides and σ phase (rich in Cr and Mo), leading to its higher susceptibility to undergo pitting corrosion compared to the ferrite phase. It follows that an increased amount and size of isothermal nitrides and σ phase will cause larger depletion in alloying elements along the α/γ boundaries and in the austenite phase, hence weaker passive film on these sites and a decreased corrosion resistance of the material. Thus the alloy composition is of critical importance for the corrosion resistance [37].

It should be noted that the 2507 ISO sample exhibited a passive behavior and good corrosion resistance in the NaCl solution at T_{room}, despite of the relatively low PRE value of the austenite phase. In a similar study of heat treated 2205 DSS, at T_{room} the sample with quenched-in nitrides in the ferrite phase exhibited a passive behavior and good corrosion resistance in 1 M NaCl solution, whereas at

exposure temperature slightly above the CPT, preferential dissolution of the austenite was observed. Also in that case the ferrite and the austenite phases had a large difference in their PRE values, with the austenite phase having the lower one. These results demonstrate the enhanced corrosiveness of the NaCl solution due to the increase of the exposure temperature, which is extensively explained elsewhere [38]. The study of the effect of the exposure temperature on the passive film formed on the ferrite and austenite phases requires advanced analytical techniques with temperature control and sufficient lateral resolution, subject for a future study.

In summary, the results from this study indicate that the presence of nano-sized quenched-in nitrides has minor influence on the corrosion/dissolution behavior of the 2507 SDSS, causing only a slight decrease in its CPT value. The presence of small isothermal nitrides and a small amount of σ phase causes a large decrease in the CPT value due to the subtraction of Cr, Mo and N, mostly from the austenite, during their nucleation and growth. Nevertheless, the corrosion resistance of the material is still good in the NaCl solution at T_{room} .

4. CONCLUSIONS

The influence of precipitated quenched-in and isothermal chromium nitrides, obtained by different special heat treatments, on the corrosion behavior of a 2507 SDSS was investigated at T_{room} and at 90 °C (above the CPT), by a combination of microstructure characterization, electrochemical polarization, in-situ electrochemical AFM measurements and post-analysis of the corroded samples. The following conclusions can be drawn:

- The isothermal nitrides (ca. 80-250 nm in size) precipitated along the α/γ boundaries, exhibiting higher Volta potential compared to the ferrite and the austenite, while a local Volta potential drop was observed at the α/γ boundaries. The Volta potential difference of the nano-sized quenched-in nitride particles (ca. 50-100 nm in size) finely dispersed in the ferrite grains could not be resolved by the KFM mapping due to their very small size.
- At T_{room} in 1 M NaCl solution, the nano-sized quenched-in or isothermal nitrides and a small amount of σ phase in the 2507 SDSS didn't cause passivity breakdown of the material. During transpassive dissolution at 1.2 $V_{\text{Ag}/\text{AgCl}}$, the ferrite phase, in the sample containing quenched-in nitrides, preferentially dissolved, whereas the α/γ boundaries in the sample with isothermal nitrides and σ phase started to dissolve.
- The nano-sized quenched-in nitrides finely dispersed in the ferrite of the 2507 SDSS have little influence on the corrosion resistance, causing a slight decrease of the CPT value. At 90 °C in 1 M NaCl solution, the sample still exhibited passive behavior up to 0.8 $V_{\text{Ag}/\text{AgCl}}$, where pitting corrosion started in the ferrite phase, likely due to some depletion in Cr and N in the ferrite matrix.
- The isothermal nitrides, together with a small amount of σ phase, precipitated in the 2507 SDSS cause a large decrease in the CPT. At 90 °C in 1 M NaCl solution the passivity was lost and a fast corrosion of the austenite occurred, probably due to depletion in Cr, N and Mo in the austenite phase caused by the precipitation of the isothermal nitrides and sigma phase along the α/γ phase boundaries.

- The results suggest that the isothermal nitrides are more detrimental than the quenched-in nitrides for the corrosion resistance of the 2507 SDSS at temperatures above the CPT. The different formation mechanisms, sizes and distributions of the quenched-in and isothermal nitrides cause different situations of alloying element depletion, and thus have different effects on the corrosion behavior of the material.

ACKNOWLEDGMENTS

AB Sandvik Materials Technology, Sweden, is acknowledged for the financial support of this study. Swerea KIMAB, Sweden, and particularly Dr. Sten Wessman are thanked for the supply of the samples. Anders Wilson at AB Sandvik Materials Technology, Sweden, is thanked for the help with the thermodynamic calculation by Thermo-Calc.

References

1. J.W. Elmer, T.A. Palmer, E.D. Specht, *Metall. Mater. Trans. A*, 38A (2007) 464
2. A.J. Ramirez, J.C. Lippold, S.D. Brandi, *Metall. Mater. Trans. A*, 34A (2002) 1575
3. T.H. Chen, J.R. Yang, *Mater. Sci. Eng.*, A311 (2001) 28
4. N. Sathirachinda, *Relative nobility of precipitated phases in stainless steels - Evaluation with a combination of local probing techniques*, KTH, Stockholm (2010)
5. IMO, *Practical guidelines for the fabrication of duplex stainless steel. Second ed*, International Molybdenum Association, London (2009)
6. O. Smuk, *Microstructure and properties of modern P/M super duplex stainless steels*, KTH, Stockholm (2004)
7. H.Y. Ha, H.S. Kwon, *Electrochim. Acta*, 52 (2007) 2175
8. J.W. Simmons, *Scr. Metall. Mater.*, 32 (1995) 265
9. J. Romu, H. Hänninen, *Mater. Sci. Forum*, 318-320 (1999) 673
10. Z.Z. Yuan, Q.X. Dai, X.N. Cheng, K.M. Chen, *Mater. Charact.*, 58 (2007) 87
11. R.F.A. Jargelius-Pettersson, *ISIJ Int.*, 36 (1996) 818
12. J. Liao, *ISIJ Int.*, 41 (2001) 460
13. Y.L. Fang, Z.Y. Liu, W.Y. Xue, H.M. Song, L.Z. Jiang, *ISIJ Int.*, 50 (2010) 286
14. N. Sathirachinda, R. Pettersson, S. Wessman, U. Kivisäkk, J. Pan, *Electrochim. Acta*, 56 (2011) 1792
15. J.-O. Nilsson, *Mater. Sci. Tech.*, 8 (1992) 685
16. P. Ferro, F. Bonollo, G. Timelli, *Metall. Ital.*, 5 (2012) 7
17. J.-O. Andersson, T. Halender, L. Höglund, P. Shi, B. Sundman, *Calphad*, 26 (2002) 273
18. N. Sathirachinda, R. Pettersson, S. Wessman, J. Pan, *Corros. Sci.*, 52 (2010) 179
19. R. Magnabosco, *Mater. Res.*, 12 (2009) 321
20. C.C. Hsieh, W. Wu, *ISRN Metallurgy*, 2012 (2012) 1
21. S. Magonov, J. Alexander, S. Wu, *Advancing characterization of materials with atomic force microscopy-based electric techniques scanning probe microscopy of functional materials*, in: A. Gruverman, S.V. Kalinin (Eds.), *Scanning Probe Microscopy of Functional Materials*, Springer, New York (2011)
22. M. Sababi, S. Ejnermark, J. Andersson, P.M. Claesson, J. Pan, *Corros. Sci.*, 66 (2013) 153
23. E. Bettini, T. Eriksson, M. Boström, C. Leygraf, J. Pan, *Electrochim. Acta*, 56 (2011) 9413
24. N. Sathirachinda, R. Pettersson, J. Pan, *Corros. Sci.*, 51 (2009) 1850
25. M. Femenia, C. Canalias, J. Pan, C. Leygraf, *J. Electrochem. Soc.*, 150 (2003) B274
26. M. Femenia, J. Pan, C. Leygraf, *J. Electrochem. Soc.*, 151 (2004) B581

27. J.-O. Nilsson, L. Karlsson, J.-O. Andersson, *Mater. Sci. Tech.*, 11 (1995) 276
28. J.-O. Nilsson, A. Wilson, *Mater. Sci. Tech.*, 9 (1993) 545
29. E.S. Rieder, X.Q. Tong, J.P.G. Farr, M. Aindow, *Brit. Corros. J.*, 31 (1996) 139
30. Y.S. Ahn, J.M. Kim, B.H. Jeong, *Mater. Sci. Tech.*, 18 (2002) 383
31. N. Ebrahimi, M. Momeni, M.H. Moayed, A. Davoodi, *Corros. Sci.*, 53 (2011) 637
32. A.M. Elhoud, N.C. Renton, W.F. Deans, *Int. J. Adv. Manuf. Technol.*, 52 (2011) 451
33. A. Bhattacharya, P.M. Singh, *Metall. Mater. Trans. A*, 40A (2009) 1388
34. J. Kruger, *J. Electrochem. Soc.*, 106 (1959) 736
35. R.S. Lilliard, *Relationship between pitting corrosion and crystallographic orientation, an historical perspective*, in: H.S. Isaacs, J.R. Scully, J.D. Sinclair, G.S. Frankel (Eds.), *Corrosion Science. A retrospective and current status in honor of Robert P. Frankenthal*, The electrochemical Society, New Jersey (2002)
36. J.-O. Nilsson, T. Huhtala, P. Jonsson, L. Karlsson, A. Wilson, *Metall. Mater. Trans. A*, 27A (1996) 2196
37. R.F.A. Pettersson, J. Flyg, *Acom*, 3 (2004) 2
38. P. Ernst, R.C. Newman, *Corros. Sci.*, 49 (2007) 3705